

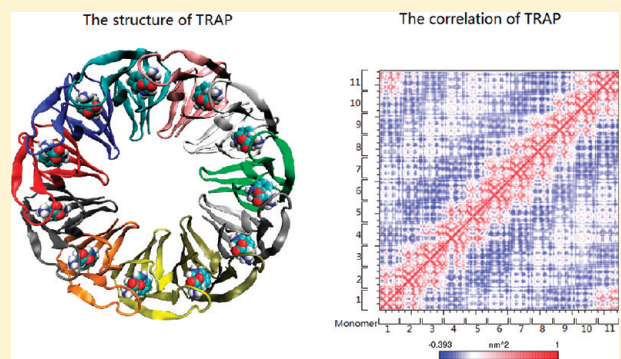
Normal Mode Analysis of Trp RNA Binding Attenuation Protein: Structure and Collective Motions

Guang Hu, Servaas Michielssens, Samuel L. C. Moors, and Arnout Ceulemans*

Department of Chemistry and INPAC Institute for Nanoscale Physics and Chemistry, Katholieke Universiteit Leuven, Celestijnenlaan 200F, B-3001 Leuven, Belgium

Supporting Information

ABSTRACT: The Trp RNA-binding protein (TRAP) has a toroidal topology and a perfect 11-fold symmetry, which makes it an excellent candidate for a vibrational study of elastic properties. Normal mode analysis in combination with correlation matrix calculations was used to detect collective low-frequency motions in TRAP. The results reveal the presence of highly correlated modes at the lower end of the spectrum, which directly reflect the annular and toroidal topology. The integral of the correlations over the low-frequency torsional part of the vibrational spectrum further demonstrates the relative rigidity of the 11 monomer building blocks of TRAP. The internal flexibility of each monomer and the effects of Trp-binding were also examined. The study clearly shows the determining influence of symmetry and topology on the elastic properties and also offers a detailed view on the Trp affinity of TRAP.



INTRODUCTION

Symmetry and topology are important in biomolecular science. Proteins may exhibit a high-symmetry and intriguing topology,¹ which often is intimately linked to a specific functionality. Toroidal proteins from a large family of DNA or RNA binding enzymes² have been shown to be essential for the DNA polymerase processivity and for the packaging of RNA and DNA through central holes as a molecular motor.³ Due to its symmetry, the formation of a toroidal structure typically involves polymerization of a fixed number of subunits, as beads in a necklace. In the present contribution, the elastic properties of such a toroidal protein are analyzed by a normal mode calculation. It will be examined to what extent the collective modes are controlled by the toroidal topology and what is the possible impact of the elastic structure on dynamic features.

As a prime model of a toroid, Trp RNA-binding attenuation protein (TRAP) was chosen. TRAP from *Bacillus subtilis* was reported to be crystallized as a complex with 11 L-Trp (Trp) molecules.^{4,5} TRAP from *Bacillus stearothermophilus* has been crystallized in complex with Trp and RNA.⁶ The TRAP molecule is a doughnut-like protein that contains 11 monomers (Figure 1a) and has exact 11-fold rotational symmetry. TRAP consists of 11 7-stranded β -sheets, each containing 4 antiparallel β -strands from one monomer and 3 β -strands from the adjacent monomer in the ring (Figure 1b). There are 11 Trp binding pockets located in between adjacent monomers. The amino and carboxyl moieties of the Trp are bound to two adjacent subunits of TRAP through eight hydrogen bonds (Figure 1c). The dynamics of TRAP such as conformational change upon binding of Trp and

RNA have been studied extensively with biochemical methods as well as with NMR spectroscopy.^{7–9} More recently Murtola et al.¹⁰ employed all-atom molecular dynamics (MD) simulation to explore the activation mechanism of Trp and RNA binding. Two main questions about the activation mechanism and the TRAP–RNA interactions were addressed.

It was proposed that Trp not only activates the protein to bind RNA but also induces a significant conformational change close to the Trp binding pockets, in particular the BC and DE loops (Figure 1b). Furthermore a principal component analysis of the molecular dynamics (MD) trajectory was used to visualize the representative fluctuations of the protein. In the present contribution both these aspects, the large-scale elasticity of the protein and the details of the Trp binding mode, will be examined using the technique of harmonic analysis. As an alternative method to MD, normal mode analysis (NMA)^{12,13} is particularly well suited for modeling large-scale motions and unraveling the molecular and dynamic mechanisms of proteins. The NMA approach has been applied successfully to not only small globular proteins, such as bovine pancreatic trypsin inhibitor (BPTI)^{14,15} and lysozyme,^{16,17} but also to larger molecular machines, such as aspartate transcarbamylase,¹⁸ ribosome,¹⁹ glycine alaph receptor,²⁰ lymphocyte function-associated antigen (LFA)-1 integrin I-domains.²¹ In recent years, coarse-grained descriptions for normal mode analysis, such as the elastic network model (ENM),^{22,23} have grown quite popular for treating very large macromolecules.

Received: June 14, 2011

Published: August 28, 2011

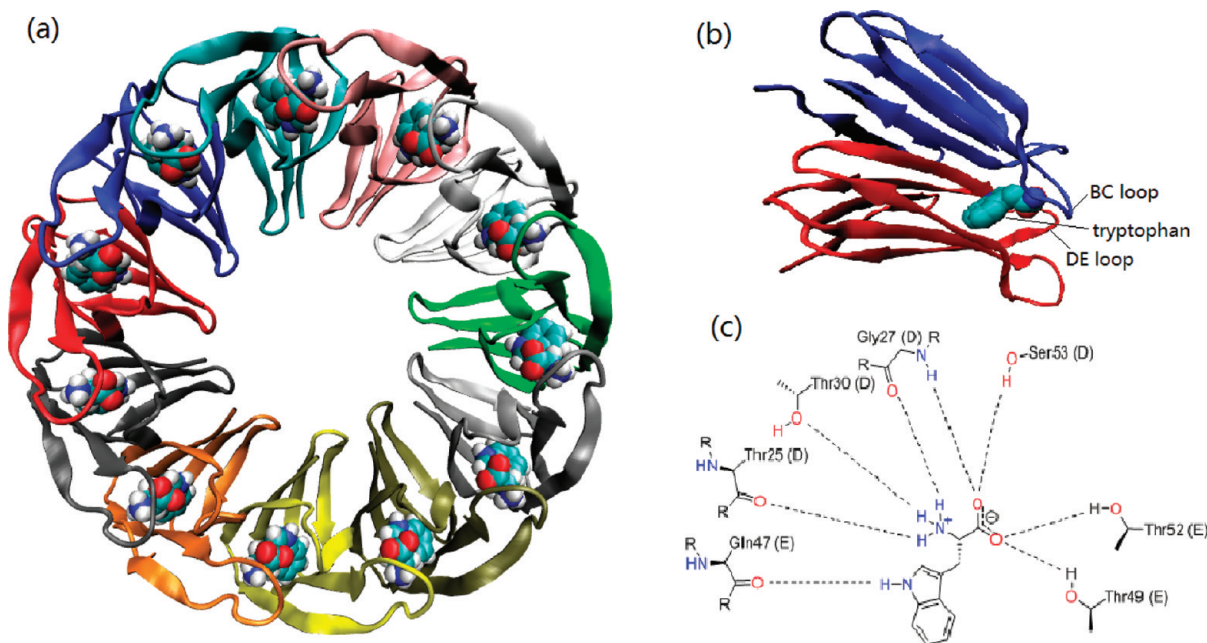


Figure 1. Toroidal structure of TRAP. (a) Cartoon representation¹¹ of the protein loaded with 11 Trps, viewed along the 11-fold symmetry axis. Each TRAP monomer is represented with a different color, and Trp atoms are shown as van der Waals spheres. (b) The Trp binding pocket located between two monomers. Each monomer contains seven antiparallel strands, three of which belong to one β -sheet and the four remaining ones to the neighboring β -sheet. The BC and DE loops are very close to the Trp binding pocket. (c) Binding of Trp to TRAP through eight hydrogen bonds.⁴

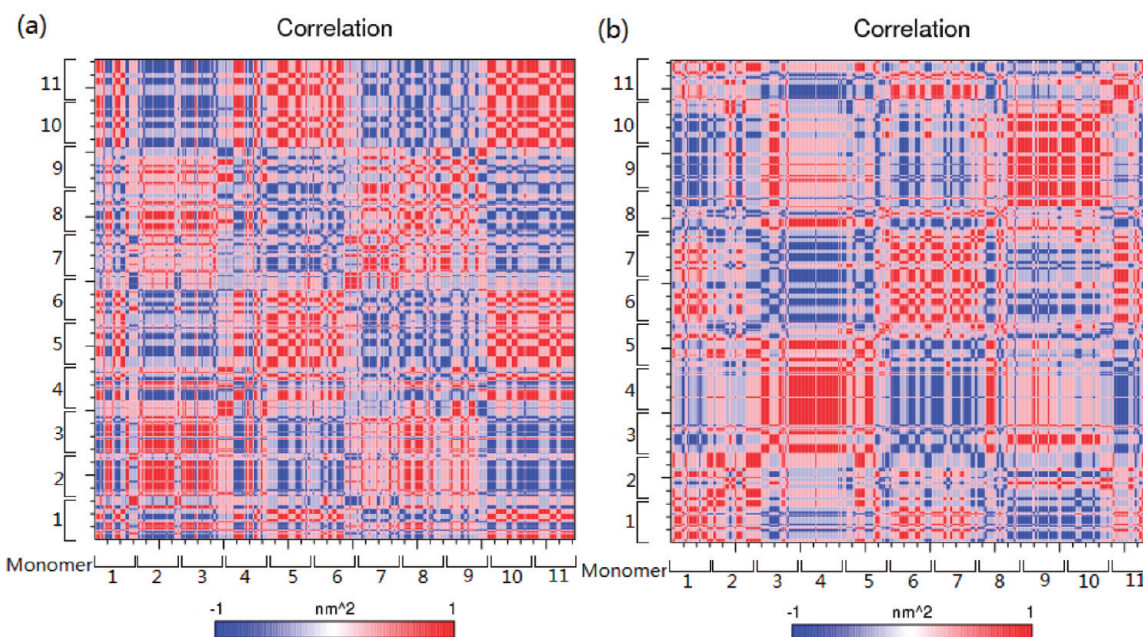


Figure 2. The correlation maps of the (a) 1st and (b) 2nd modes. The protein is divided into four domains according to correlated motions. Although all monomers are identical, the numbers show that they belong to different domain motions.

Low-frequency modes are mainly governed by the shape of the biological molecules.^{24,25} These so-called soft modes are of particular importance as presumable indicators of large-scale conformational changes which relate to the functionality of the protein. Hence it is interesting to investigate especially the low-frequency dynamics of proteins with a particular geometry and topology. It often comes as a surprise that a straightforward

harmonic analysis of a protein in crystal geometry may reveal the dominant elastic features which determine the biologically interesting conformational changes. Symmetry-based applications of NMA and ENM have been performed to investigate the molecular motions of cylindrical proteins^{26,27} and of icosahedral virus capsids,^{28,29} which are among the largest spherical proteins. The vibrations of the capsids have also been analyzed

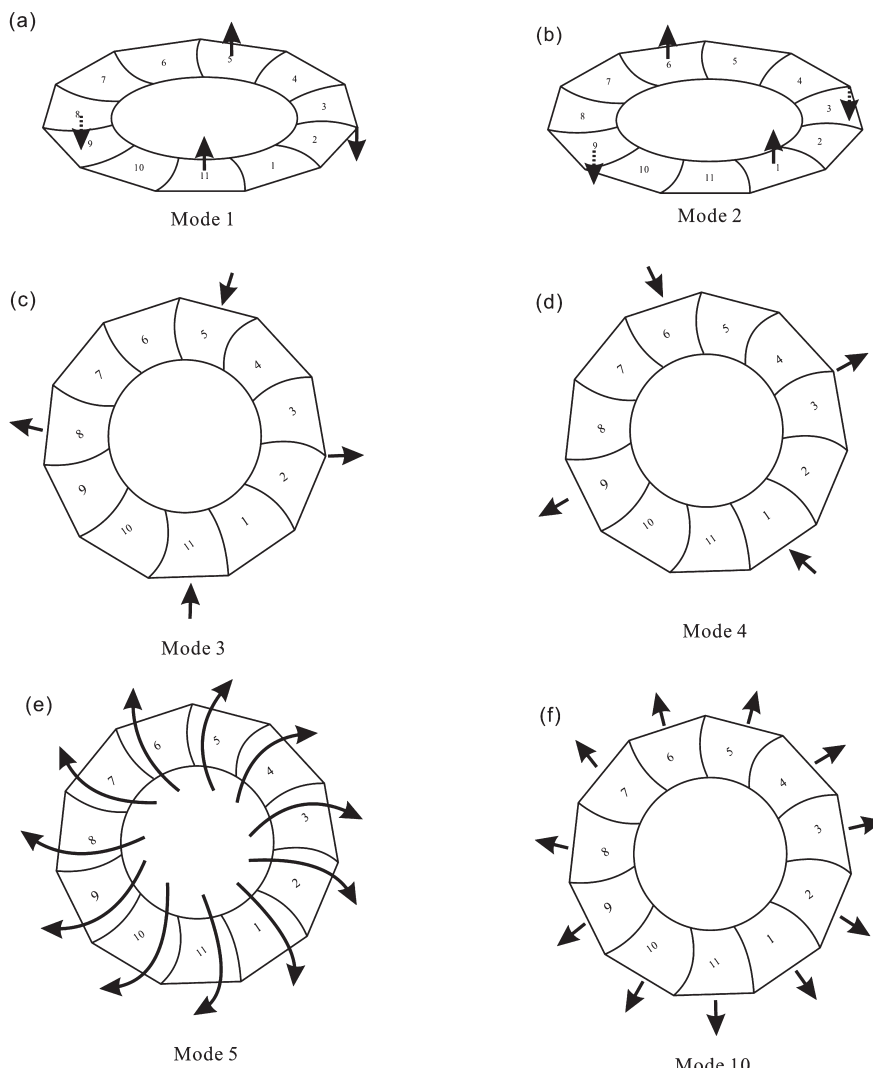


Figure 3. The out-plane motions of (a) the 1st mode located at 2.1 cm^{-1} and (b) the 2nd mode located at 2.2 cm^{-1} . The quadrupolar in-plane motions of (c) the 3rd mode located at 2.7 cm^{-1} and (d) the 4th mode located at 2.8 cm^{-1} . (e) The ‘anapolar’ motion of the 5th mode located at 3.1 cm^{-1} and (f) the breathing motion of 10th mode located at 4.7 cm^{-1} , which are generated by ENM. Arrows indicate directions of the motions.

from the point of view of group theory constraints.^{30–32} The results of these studies show that in the low-frequency range, both types of protein behave like continuous elastic bodies.

The present research focuses on how toroidal topology and symmetry affect large-scale motions. To this aim NMA is applied to TRAP as a suitable model system. The low-frequency correlated motions along selected individual normal modes are investigated in detail, and also integrations over the torsion region of the spectrum are performed to access the vibrational protein dynamics over the whole frequency range.³³ The effects of Trp binding are also discussed by comparing TRAP with and without 11 Trp molecules. The NMA results are discussed from the viewpoint of molecular topology and molecular dynamics.

METHODS

NMA Calculation. The TRAP crystal structure (PDB code: 1WAP) consists of 740 amino acid residues. After adding missing hydrogen atoms, the total numbers of atoms without and with

Trp are 11 583 and 11 880, respectively. Normal mode calculations were performed on TRAP both with and without Trp. The program Gromacs³⁴ (version 4.5.2, double precision) with the Amber03 force field³⁵ was used for all the protein simulations. The Trp parameters were taken from the Amber 6 software package.³⁶

The actual calculation of the vibrational spectrum is preceded by an energy minimization. A shift function with cutoff at 10 Å was used for the electrostatics and van der Waals interactions. Initial optimization was done with a steepest descent algorithm and continued until the absolute maximal force was smaller than 100 kJ/(mol·nm). The system was further relaxed by conjugate gradient algorithm to a maximal absolute gradient of 1 kJ/(mol·nm) and finally using low-memory Broyden–Fletcher–Goldfarb–Shanno (L-BFGS) quasi-Newtonian optimization to an maximal absolute gradient of 2.62×10^{-9} kJ/(mol·nm). After energy minimization, the root-mean-square deviations of protein backbone with respect to the crystal structure are 0.9 and 1.2 Å with and without Trp, respectively. Subsequently one calculates the Hessian matrix, which is the matrix of

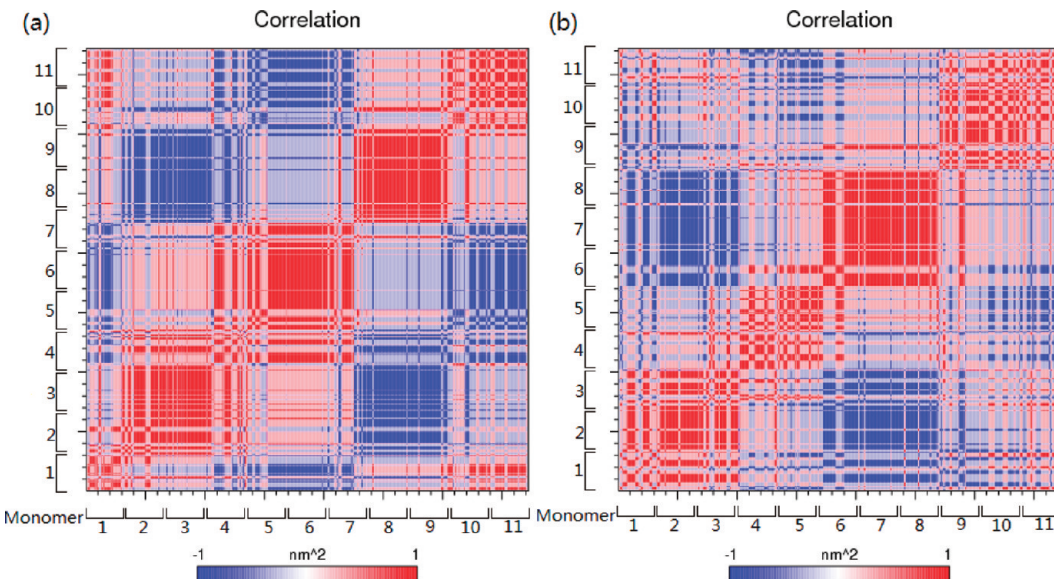


Figure 4. The correlation maps due to the (a) 3rd and (b) 4th modes.

second derivatives of the potential energy with respect to the mass-weighted atomic coordinates. Diagonalization of this matrix yields the eigenvalues Ω and eigenvectors \mathbf{W} (the normal modes), which include the six spurious translations and rotations at zero energy. The frequencies of the first 4 modes are exactly 0, while the remaining 2 are almost 0 (0.0017 and 0.0027 cm^{-1}).

ENM Calculation. The all-atom ENM calculation was performed on the minimized structure with the NOMAD-ref program.³⁷ The cutoff distance and distance weight were set at 8 and 5 Å, respectively, and a sparse matrix representation of the Hessian matrix was used to reduce memory requirements.

Correlation Analysis. The correlation matrix, \mathbf{C} , can be readily calculated based on the eigenvalues and eigenvectors:³⁸

$$\begin{aligned} \mathbf{C}_{ij} &= \frac{\langle \Delta x_i \Delta x_j \rangle}{\langle \Delta x_i \Delta x_i \rangle^{1/2} \langle \Delta x_j \Delta x_j \rangle^{1/2}} \\ &= \frac{\sum_{l=1}^n \frac{\mathbf{W}_{il} \mathbf{W}_{jl}}{\Omega_l}}{\left(\sum_{m=1}^n \frac{\mathbf{W}_{im} \mathbf{W}_{im}}{\Omega_m} \right)^{1/2} \left(\sum_{n=1}^n \frac{\mathbf{W}_{jn} \mathbf{W}_{jn}}{\Omega_n} \right)^{1/2}} \quad (1) \end{aligned}$$

where Δx_i and Δx_j indicate components of the mass-weighted displacement vectors of any two atoms or residues i and j , Ω_l denotes the mass-weighted Hessian eigenvalue of the l^{th} mode, and \mathbf{W}_{il} is the (normalized) eigenvector coefficient of atom or residue i in mode l . The summation is over a given n -dimensional subspace of the normal mode spectrum, such as $n = 2$ and 100 in our study. Integral correlations are sums of the correlations individual normal modes over a particular spectral range.³³ It should be noted that the correlation matrix of MD can be calculated by the displacement vectors directly. When treating residues, we take C_α carbons to replace the residues. For completely correlated motions, $\mathbf{C}_{ij} = 1$, and, for completely anticorrelated motions, $\mathbf{C}_{ij} = -1$. There is no correlation when $\mathbf{C}_{ij} = 0$.

Convergence of Correlation Matrices. The Euclidean norm of a matrix is the Euclidean length that gives a measure of the

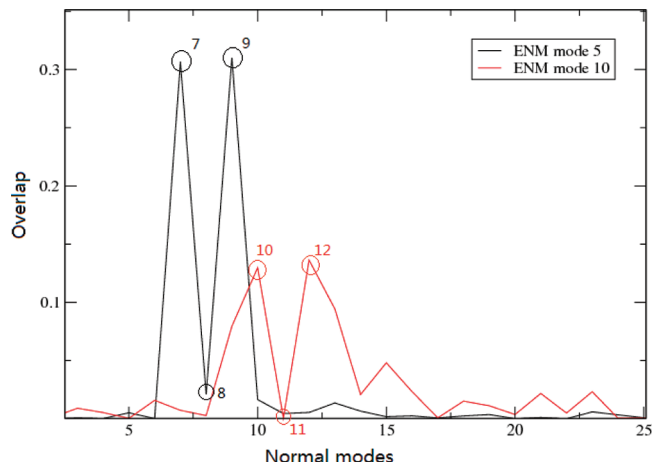


Figure 5. The overlap of the 5th (the black line) and 10th (the red line) ENM modes with the 25 lowest NMA modes.

magnitude to the elements of the matrix. For a correlation matrix \mathbf{C} , its Euclidean norm $\|\mathbf{C}\|_e$ is defined as

$$\|\mathbf{C}\|_e = \left(\sum_{i=1}^n \sum_{j=1}^n C_{ij}^2 \right)^{1/2} \quad (2)$$

The Euclidean norm has been used to test the convergence of a correlation matrix, which estimates how many normal modes are needed to describe the correlated motions of a protein.³⁹ The upper limit for the Euclidean norm is reached when all motions are fully correlated. When limited to the residues this value equals 740.

Flexibility Analysis. The flexibility was described in terms of the root-mean-square fluctuations (RMSF).^{40,41} The fluctuation of the i^{th} atomic coordinate, Δx_i , can be calculated from the eigenvectors and eigenfrequencies:

$$\langle \Delta x_i^2 \rangle = \frac{k_B T}{m_i} \sum_{l=1}^n \frac{\mathbf{W}_{il}^2}{\omega_l^2} \quad (3)$$

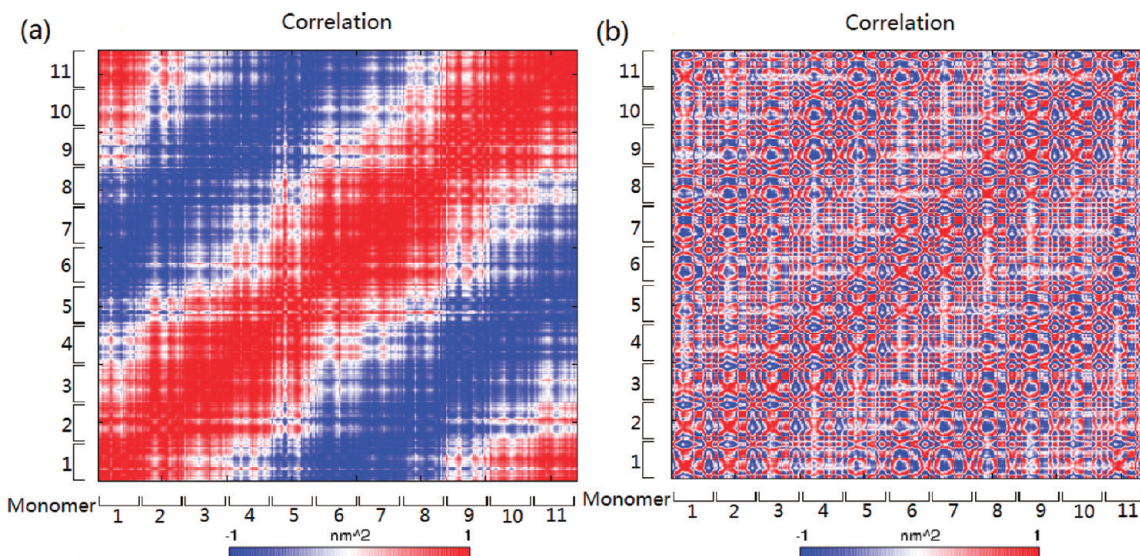


Figure 6. The correlation maps the (a) breathing and (b) anapolar modes. The correlations generated by ENM show the elastic feature of the protein.

where m_i is the mass of the atom corresponding to the i^{th} atomic degree of freedom, k_B is Boltzmann's constant, the temperature T in the simulation is 300 K, n is the number of normal modes included, and \mathbf{W}_{il} is the i^{th} component in the l^{th} eigenvector with frequency ω_l , with $\Omega_l = (2\pi\omega_l)^2$. Residue-based fluctuations are averages over all atoms in the residue.

Comparison of NMA and ENM. To quantify the similarity between the normal and ENN mode vectors, the overlap between the k^{th} ENM mode and the l^{th} NMA mode was calculated by⁴²

$$S_{kl} = \sum_{i=1}^{3N} \mathbf{U}_{ik} \mathbf{W}_{il} \quad (4)$$

where the columns of \mathbf{U} and \mathbf{W} are the respective eigenvectors. By definition, a larger overlap indicates that the two modes are highly similar and that the cumulative sum of the squared overlaps is equal to one.

RESULTS

Collective motion in a protein is any motion that involves a number of atoms moving in a concerted fashion. Such modes are known to play an important role in protein function.⁴³ To visualize these modes, we calculate the correlation coefficients and plot them in correlation maps. In the map, red indicates the highly correlated motions, blue represents the anticorrelated motions, and white is for the uncorrelated motions. These maps can refer to individual modes but may also be used to visualize a superposition of modes over a certain spectral range. All data shown are derived from all-atom normal mode analysis unless mentioned otherwise.

Global Ring and Toroid Modes. The lowest frequency modes often show the highest correlations. This means that they describe highly collective motions which reflect the most flexible distortions of the protein. This is indeed the case for the four lowest modes in TRAP at frequencies of 2.1, 2.2, 2.7, and 2.8 cm⁻¹, respectively. The correlation maps show that the protein is divided into four parts, which correspond to domain motions, as shown in Figures 2 and 3. The correlation map represents the collective behavior of domains as well as the correlation of motions between domains. For the first mode,

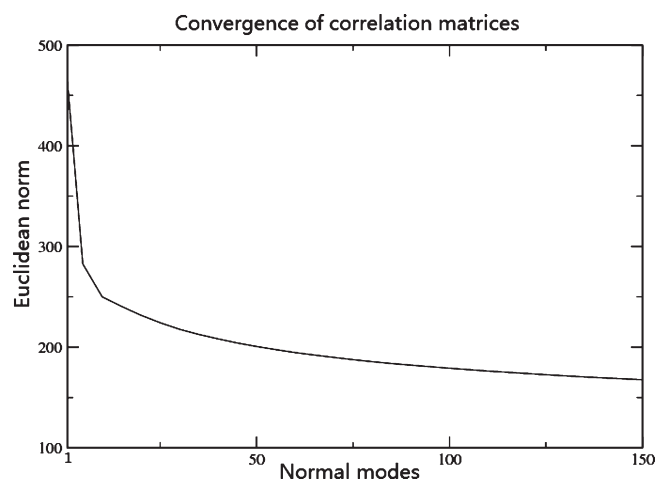


Figure 7. Euclidean norms of correlation matrices with an increasing number of normal modes. The convergence of matrices is obtained at ~ 100 normal modes.

which is the ground level of the vibrational spectrum, the four domains correspond to monomers 2–3, 4–5–6, 7–8–9, and 10–11–1. For the second mode, the four domains consistently shift one monomer, to monomers 3–4, 5–6–7, 8–9–10, and 11–1–2. Adjacent domains are anticorrelated, while opposite domains are fully correlated. The separation in four domains points to the quadrupolar character of these modes. Indeed as shown in Figure 3a and b, these modes simply correspond to the two components of the out-of-plane saddle distortion, which is recognized as the ground level in the elastic model of a vibrating ring. The softest motion of TRAP thus reflects its essential circular topology.

For the third and fourth modes, the protein is again divided into four domains, as can be seen in Figures 3 and 4. The domains are determined by symmetry breaking from perfect cylindrical symmetry. As can be seen from the figures, the domains for modes 3 and 4 are the same as for modes 1 and 2. However correlations between domains are reversed as compared to the ground modes: adjacent domains are weakly correlated, while opposite domains are strongly anticorrelated. This corresponds

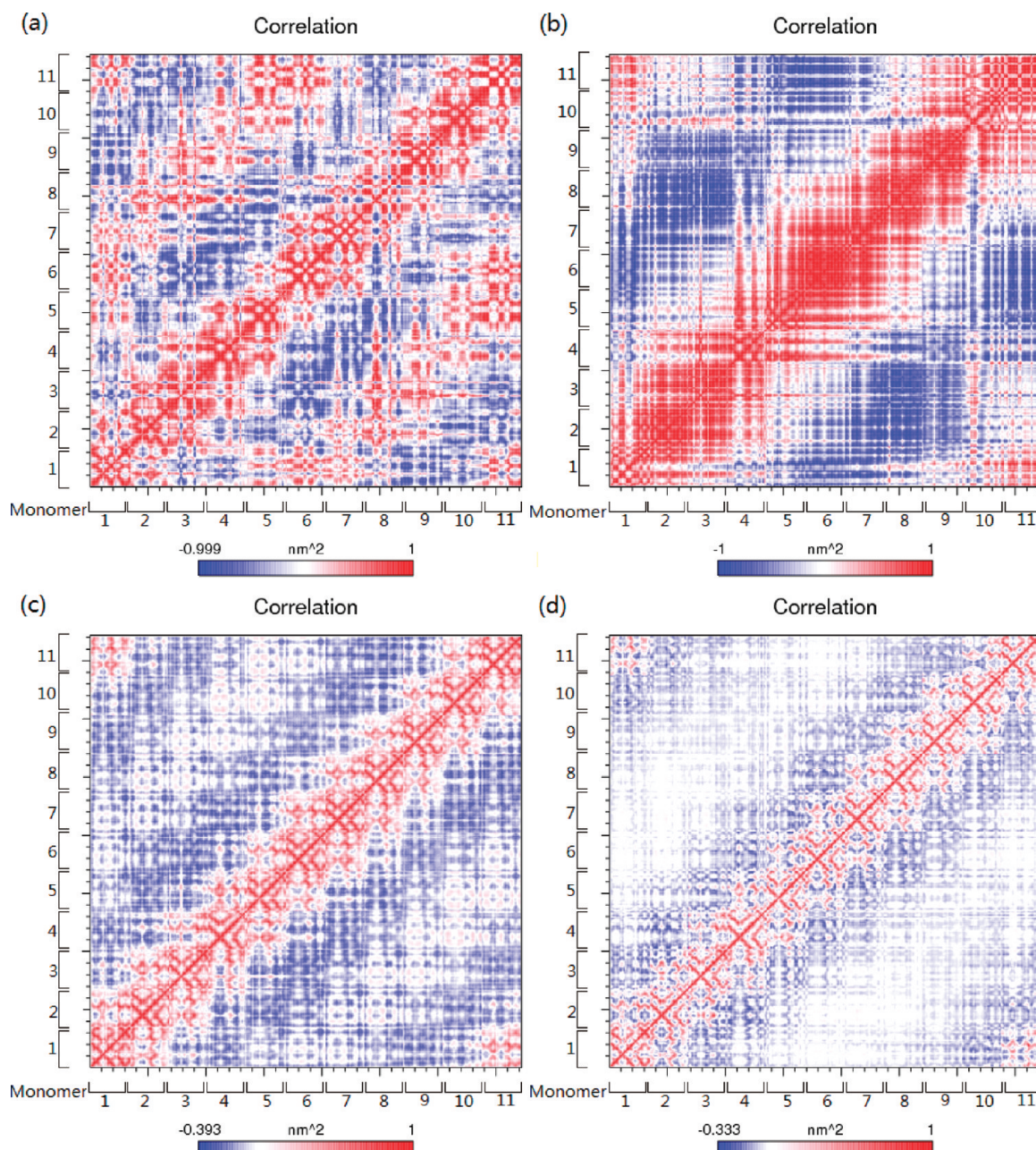


Figure 8. The correlation maps of four subspaces show the circular 11-fold symmetry on diagonal blocks. (a) Superposition of the correlation maps of 1st and 2nd and (b) of 3rd and 4th modes, and (c) the correlation map integrated over the subspace from mode 1 to 100 and (d) the subspace from mode 5 to 105.

to the distortions depicted in Figure 3c and d. They describe in-plane bendings of quadrupolar character, which transform as the harmonic functions x^2-y^2 and xy . They are the ground level of a separate class of annular vibrations.⁴⁴ Their appearance at the bottom of the vibrational spectrum demonstrates that the low-frequency region of the spectrum is controlled by the circular topology of the toroid.

Besides out-of-plane and in-plane bendings, elastic rings are also characterized by a separate class of stretching vibrations.^{44,45} The ground level of this class is the totally symmetric breathing mode. It is expected at higher frequencies than the bending modes. Unfortunately, in the all-atom normal mode analysis this mode is not easy to detect, because of mode mixing. This mode

mixing may be ascribed to the principle that all-atom NMA takes into account the detailed chemical structures that distinguish a toroidal protein from a mechanical ring. To detect this breathing motion we have made use of ENM. Since ENM is a coarse-grained model, it removes the atomistic details of NMA and enhances the collective character of the soft modes. This analysis easily retrieves the breathing mode as the 10th mode at 4.7 cm^{-1} (Figure 3f). Another interesting collective motion appears at the fifth mode. Along this mode, the toroidal molecule follows a poloidal coordinate (Figure 3e). The fifth mode is the 'anapolar' vibration, which is typical of toroidal topology and has no counterpart in rings.⁴⁶ To estimate the positions of these two modes in NMA, the overlaps between the fifth and 10th ENM

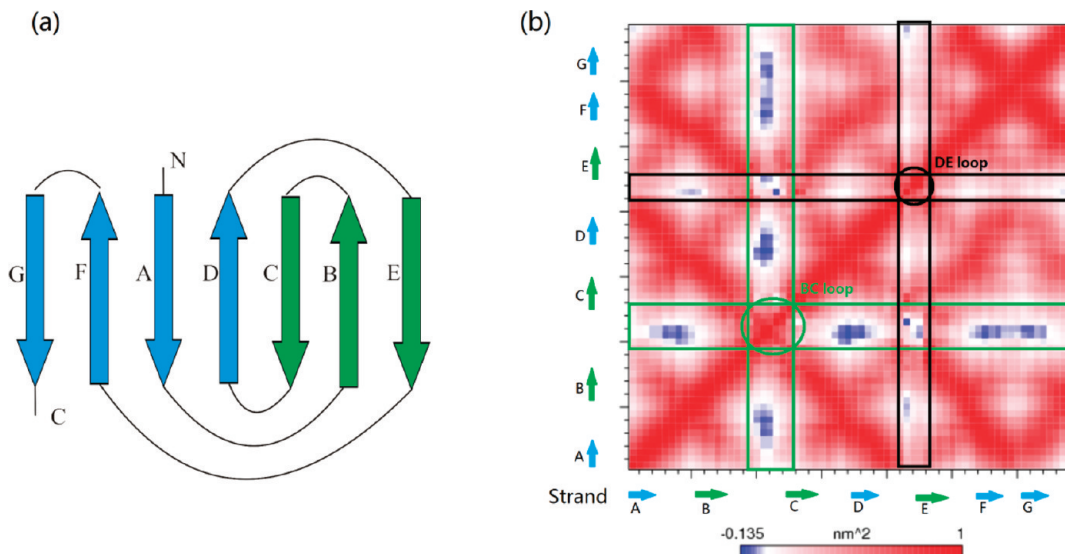


Figure 9. (a) Schematic representation of one monomer, and (b) its correlation map integrated over the first to 100th modes. The correlated motion of the BC loop and the DE loop are highlighted in green and black boxes.

mode with the 25 lowest NMA modes were calculated. Figure 5 indicates that the two modes are still localized in the low-frequency region of the NMA spectrum. The eighth to 10th and 12th to 14th NMA modes give substantial contributions to the breathing mode, whereas the 11th mode has no contribution because it is antisymmetric. A similar result is found for the anapolar mode.

In Figure 6 two correlation maps illustrate the correlated motions of the totally symmetric and the anapolar modes, respectively. For the totally symmetric mode, the diagram shows a typical monotonic change of full correlation (+1) to full anticorrelation (-1), corresponding to a half-turn around the ring. Individual subunits are not visible here, and the whole protein moves in a concerted manner just as an elastic continuum. For the anapolar mode, all residues are divided into an upper and a lower layer, which move oppositely. Residues within each layer have highly correlated motion, while the relative motions of the layers are anticorrelated: One is moving inward and the other outward. This leads to a highly fragmented correlation map.

Integral Correlations. In the previous section, we studied the dynamics of a few normal modes with very low frequency individually. However Ichiye and Karplus³⁷ have argued that a large number of low-frequency NMA modes are required to realize the correlated motions of a protein. To estimate the convergence of the normal modes, the Euclidean norms of the correlation matrices (see Methods Section) were calculated with an increasing number of normal modes. The result is shown in Figure 7.

Figure 7 illustrates the dramatic change in Euclidean norms due to only a very small number of normal modes included. In particular, the curve drops down from the first to fifth modes, which means that first five modes are not enough to achieve the convergence of correlations. When a larger number of modes is included, the curve becomes much smoother and remains stable above ~ 100 modes. Therefore, we investigate correlations which are integrated over different subspaces at low frequency. First of all we have simply taken the superposition of the lowest out-of-plane modes 1 and 2 (Figure 8a). This superposition shows

almost perfect annular symmetry, which proves that these two modes are the components of a degenerate cylindrical level. An entirely similar result is obtained in Figure 8b for the superposition of modes 3 and 4, which are the components of the in-plane quadrupolar level.

In Figure 8c we have integrated the correlation diagrams over the first 100 modes, and in Figure 8d we have taken the range from mode 5 to 105. The comparison of both diagrams clearly illustrates the dominant influence of the four softest modes in the correlated motion. The diagrams clearly show that the TRAP has 11 modules, which each relate to 1 monomer. Thus, the remarkable symmetry of TRAP is evident in the correlation maps. In a correlation map, the intramonomer correlations are marked on diagonal blocks, while the intermonomer correlations are represented on off-diagonal blocks. Of all correlated motions, the intramonomer and—to a lesser extent—nearest neighbor correlations are the strongest. The reason for this lies in the way TRAP is constructed. The hydrophobic core located between the two partial β -sheets keeps the overall shape of each monomer intact, whereas adjacent monomers are connected by strong hydrogen bonds between two neighboring β -strands, thereby allowing limited flexibility between them.

Topology of a Single Monomer. Each monomer contains seven β -strands, with three β -strands in one plane and four β -strands in another plane. In Figure 9a, the seven β -strands on two planes are plotted by different colors. As can be seen in Figure 9c, the correlation patterns of the 11 monomers are very similar. As discussed in the above section, extension of the correlation to the first 100 modes is sufficient to describe collective dynamics, up to the level of secondary structures. Therefore, we zoom in on the correlation of a single monomer for this subspace (Figure 9b).

The five pronounced stripes perpendicular to the diagonal indicate that the strongest correlations exist between neighbor strands in the same plane, A and D, A and F, B and C, B and E, F and G. The three weaker lines parallel to the diagonal indicate that the second strongest correlations are between strand D and F and A and G. These correlated motions may be caused by hydrogen bonds between β -strands or close packing between

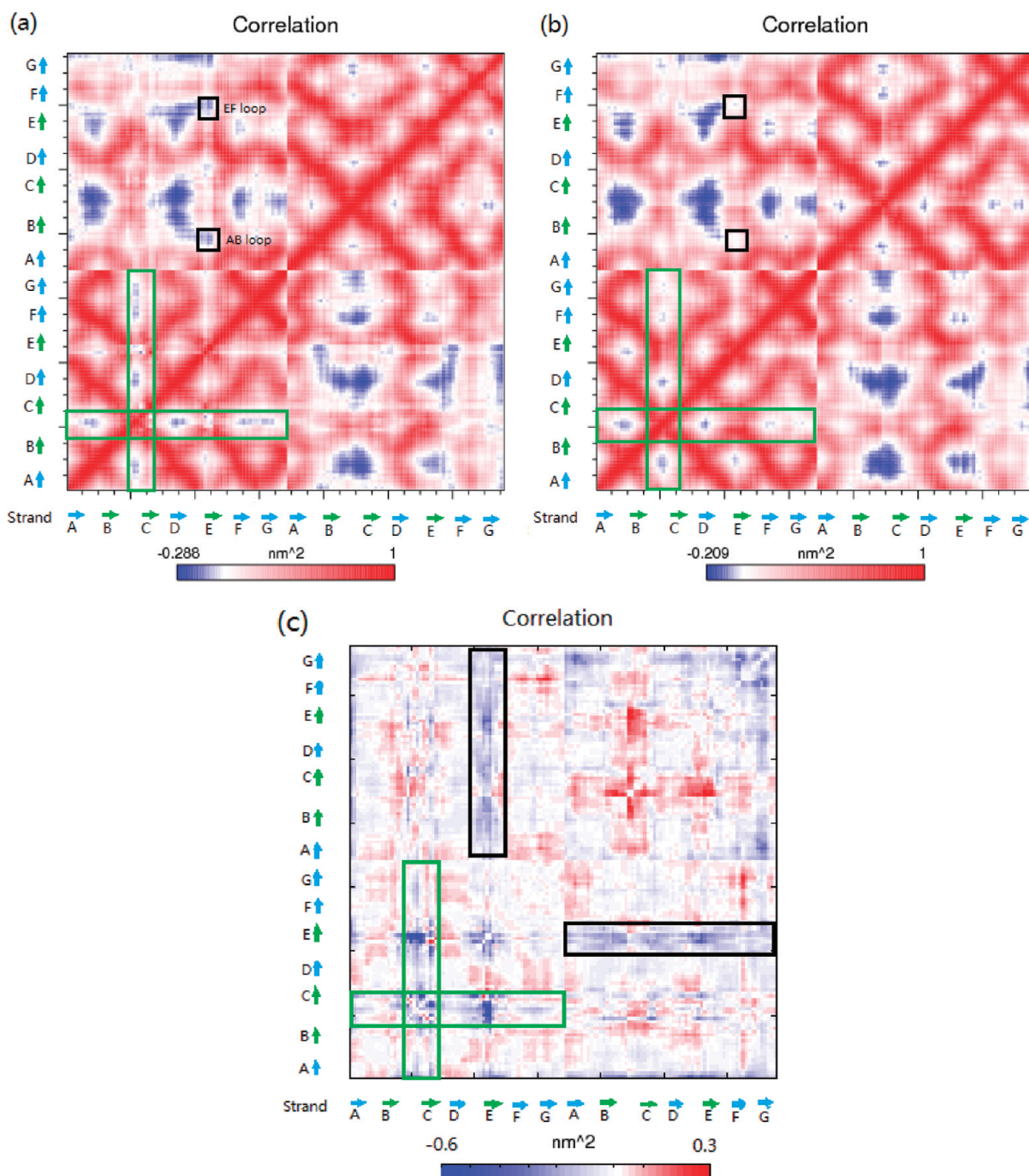


Figure 10. The correlation maps, integrated over modes 1–100, of 2 adjacent subunits (a) without and (b) with Trp binding and (c) their difference matrix. Two highly anticorrelated clusters of residues are marked by boxes, which are close to the Trp binding pocket.

β -sheets. The green and black boxes represent the correlation of the flexible BC and DE loops, respectively. The BC loop shows an anticorrelation, and the DE loop has almost no correlation with other residues, which indicates that the motions of both loops are largely independent of the rigid domain defined by the two β -sheets. Therefore, the correlation within each monomer of TRAP clearly reflects its secondary structure. In summary, the relative flexibility of the whole protein shown as four different domain motions in the low-frequency modes is the result of quadrupolar symmetry breaking of a protein, which behaves as an elastic rod. Investigation of a single monomer at higher

frequencies reveals that the correlations of a monomer are controlled by its β -sheet secondary structure, while the correlations of the whole protein depend on its topology and symmetry.

Effects of Tryptophan Binding. Both experiments and molecular dynamics analysis have been used to investigate the effects of Trp binding on the dynamic properties of TRAP.^{4,10} Here, we study the effects of Trp with NMA.

The presence of Trp reverses the ordering of modes 1 and 2, but since these modes belong to one degenerate cylindrical mode, a very small distortion is enough to invert the symmetry breaking. However, Trp binding has little effect on the integrated

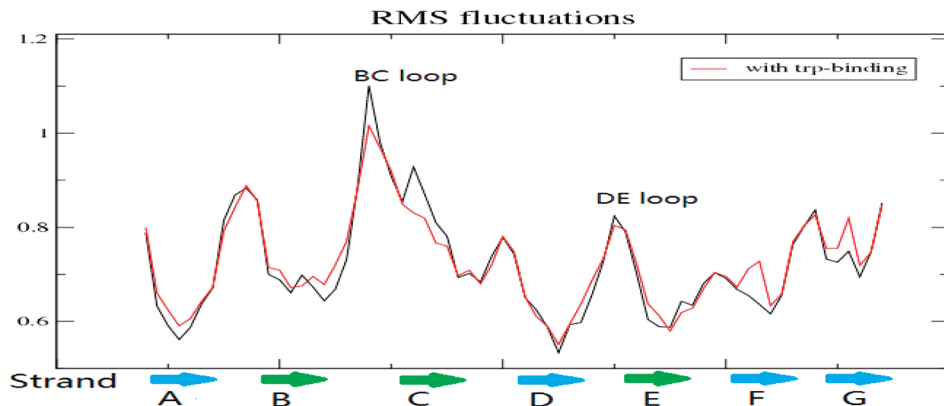


Figure 11. The backbone RMSF of TRAP with (the black line) and without (the red line) Trp, based on the full set of normal modes.

dynamics of the protein, which is not unexpected, since the toroidal topology remains intact. This verifies that the low-frequency motions of a macromolecule are mostly decided by its shape. Upon closer examination a larger effect is predicted for the dynamics of the interface between two adjacent subunits, which is located at the Trp binding pocket. As highlighted in green boxes in Figure 10, the anticorrelation between the BC loop and other intramonomer residues is reduced in the presence of Trp. The black boxes show a similar effect for the anticorrelations between the DE and the AB and EF loops of the adjacent subunit. The motions of the BC and DE loops are more strongly correlated with those of nearby residues in the presence of Trp, which indicates that these loops are now part of a rigid domain. As shown in Figure 10c, these effects are visualized more clearly in the correlation difference map, which is obtained by the correlation matrix without Trp minus the correlation matrix with Trp.

To further investigate the influence of Trp binding on flexibility, the comparison of the RMSF of the full set of normal modes between TRAP with and without Trp is shown in Figure 11. The fluctuation profile for both systems is very similar. Regions with high residue fluctuations are mostly localized to the loops connecting the β -strands and the loops at the chain termini. The highest fluctuations are found in the large BC loop, which acts as a covering lid for the Trp at the outside of the protein. Slight differences between the two systems are found in the BC loop. This is in agreement with the RMSF result in the previous MD simulation.¹⁰ In addition, two other obvious effects are observed at β -strands C and F. The lower flexibility of β -strand C in the presence of Trp is easy to understand because this β -strand is in the vicinity of the Trp binding pocket, whereas the higher flexibility of β -strand F may be caused by the steric effect of the neighboring Trp.

■ DISCUSSION

Global Toroidal Topology and Existence of Ring Modes.

A vibrating ring has three separate classes of vibrations: out-of-plane motions, in-plane bending, and in-plane stretching.⁴³ In each class the vibrational frequency increases with an integer cylindrical quantum number, λ . For the out-of-plane class, the lowest angular mode is quadrupolar ($\lambda = 2$). The monopole ($\lambda = 0$) and dipolar ($\lambda = 1$) motions simply correspond to the upward translation and perpendicular rotations, respectively, and thus are frequency-less. The second class starts out at a bit higher energy,

again with a quadrupolar mode. In this case, the monopole and dipole are the cylindrical rotation and the in-plane translations. In this way all six spurious modes are removed. Consequently the third class starts out at the monopolar ($\lambda = 0$) mode, which corresponds to the totally symmetric breathing mode. As this involves ring stretching, it will be located at higher energy. Clearly the onsets of these three classes are present in the low-frequency domain of our toroidal protein, and symmetries and energy ordering is as expected from the ring model. This confirms that the softest modes of such macromolecules reflect the overall circular topology of the structure. On a finer scale, we also detected the anapolar collective mode which is typical for a torus.⁴⁷

Comparison with Molecular Dynamics and NMR. MD and NMA are two commonly used methods to study the dynamics of proteins. MD, based on statistical mechanics, can give an accurate simulation of protein motion over a certain time interval, while NMA adopts harmonic potential models. Many comparative studies of MD and NMA have been published in the literature.^{48–50} Quite remarkably, NMA seems to predict quite well the RMSF values of the global dynamics, for a fraction of the computational cost of a full MD simulation.³⁸

Murtola et al.¹⁰ applied principle component analysis (PCA) on MD trajectories to determine the important conformational changes of TRAP. For the TRAP without Trp (apo-TRAP), the largest motions were associated with the loops near the Trp binding site, especially the BC loop. This is also confirmed by the RMSF analysis (vide infra). Interestingly for the TRAP with Trp (holo-TRAP), the largest mode is a ring deformation mode. Clearly this result can be projected onto the low-frequency spectrum obtained by NMA. As compared to NMA, the PCA method is based on an ensemble which is not limited to one local minimum and in this way also includes anharmonic motions between the wells. Nevertheless simple harmonic analysis correctly identifies the conformational flexibility of the protein. It offers in addition a deconvolution of the global modes, based on symmetry and topology.

An interesting comparison can also be made with the NMR results by McElroy et al.⁹ Although the TRAP protein in their study is from another bacterium (78% sequence identity), the RMSF spectrum in Figure 11 compares favorably with their results. In particular, Figures 3c and d in their paper show that the resonance line widths, which are related to the dynamics on the micro- to millisecond time scale, are highest for the residues closest to the Trp binding site: 23–37 and 47–56.

This corresponds nicely with our Figure 11. Without Trp, the lines of these residues are broadened beyond detection in the apo-TRAP spectrum. For residues 23–37, this is in agreement with a higher RMSF for apo-TRAP in Figure 11. However, for residues 47–56, the difference between apo- and holo-TRAP is not evident from the RMSF (though there is evidence of this in the difference matrix). The line broadening for residues 60–67, which are far from the Trp binding pocket, suggests that Trp mediates allosteric regulation of RNA binding by TRAP. This is confirmed in our NMA analysis by the increased RMSF in this region but not evident from the MD simulation.

Trp Binding Pockets. Each of the 11 Trp molecules locates at a pocket between 2 adjacent subunits.⁶ The evident similarity of the correlations between TRAP with and without Trp shows that the overall dynamics of the protein are maintained, independent of whether the Trp is bound or not. However, the Trp binding mostly modifies the BC and DE loop correlation behavior. The anticorrelations of the BC loop, as well as the DE loop, become significantly weaker upon Trp binding. Our NMA results indicate that the protein is more rigid upon Trp binding, in line with the general conclusions from NMR and MD.^{9,10} The observation of monomer blocks in the correlation maps indicates that the basic collective modes can be reproduced by the mobile block Hessian method.^{51,52} This approach is not suitable though to study the Trp binding modes, which depend on the internal flexibility of the blocks and the intermonomer interactions.

CONCLUSIONS

In this article, we have reported the normal mode analysis simulations of TRAP. It is observed that the long-range deformations of this molecule comply with the lowest vibrational excitations of elastic continua with the same toroidal topology. Correlations over the low-energy torsional part of the spectrum further reveal the clear 11-fold symmetry of the monomeric building blocks. Hence there are two rules that govern the correlated motions: First, the toroidal topology plays a dominant role in the correlated motion of the lowest frequency modes. Second, integral correlations over the low-frequency part of the vibrational spectrum are decided by the 11-fold symmetry.

The correlation of the secondary structure β -sheet shows that it has significant rigidity. Effects of Trp binding also suggest that low-frequency modes are always decided by molecular shape. We hope this study of how toroidal topology and symmetry affect large-scale motions will be useful to analyze low-frequency dynamics⁵³ of macromolecules with high-symmetry¹ and nonplanar topologies.²

To fully understand how the dynamics define its function, a confrontation between NMA and the biochemical process of TRAP binding to RNA is needed. To achieve this aim, the NMA method should be extended to the TRAP–RNA complex. In this way, the following two issues could be investigated: (1) To find out which modes play an important role in the binding of RNA molecules. In previous studies, the “blossoming-like” motion⁴⁵ and the quaternary twist motion⁵⁴ have been suggested to contribute to the gating mechanism for the ligand-gated ion channels.⁵⁵ (2) To find out how the Trp affects the RNA-binding motion mode.

ASSOCIATED CONTENT

Supporting Information. MPEG movies of four low-frequency vibrational modes of TRAP. This information is available free of charge via the Internet at <http://pubs.acs.org/>.

AUTHOR INFORMATION

Corresponding Author

*E-mail: Arnout.Ceulemans@chem.kuleuven.be.

ACKNOWLEDGMENT

Financial support from the Flemish Government through the concerted action scheme is gratefully acknowledged. G.H. thanks INPAC for a postdoctoral fellowship. S.M. is doctoral fellow of the FWO Science Fund.

REFERENCES

- (1) Goodsell, D. S.; Olson, A. J. Structural symmetry and protein function. *Annu. Rev. Biophys. Biom.* **2000**, *29*, 105–153.
- (2) Hingorani, M. M. O’Donnell, M. Toroidal proteins: running rings around DNA. *Curr. Biol.* **1998**, *8*, R83–R86.
- (3) Mancini, E. J.; Kainov, D. E.; Grimes, J. M.; Tuma, R.; Bamford, D. H.; Stuart, D. I. Atomic snapshots of an RNA packaging motor reveal conformational changes linking ATP hydrolysis to RNA translocation. *Cell* **2004**, *118*, 743–755.
- (4) Antson, A. A.; Otridge, J.; Brzozowski, A. M.; Dodson, E. J.; Dodson, G. G.; Wilson, K. S.; Smith, T. M.; Yang, M.; Kurecki, T.; Gollnick, P. The structure of Trp RNA-binding attenuation protein. *Nature* **1995**, *374*, 693–700.
- (5) Chen, X.-P.; Antson, A. A.; Yang, M.; Li, P.; Baumann, C.; Dodson, E. J.; Dodson, G. G.; Gollnick, P. Regulatory features of the Trp operon and the crystal structure of the Trp RNA-binding attenuation protein from *Bacillus stearothermophilus*. *J. Mol. Biol.* **1999**, *289*, 1003–1016.
- (6) Antson, A. A.; Dodson, E. J.; Dodson, G.; Greaves, R. B.; Chen, X.-P.; Gollnick, P. Structure of the Trp RNA-binding attenuation protein, TRAP, bound to RNA. *Nature* **1999**, *401*, 235–242.
- (7) Li, P. T. X.; Scott, D. J.; Gollnick, P. Creating hetero-11-mers composed of wild-type and mutant subunits to study RNA binding to TRAP. *J. Biol. Chem.* **2002**, *277*, 11838–11844.
- (8) Li, P. T. X.; Gollnick, P. Using hetero-11-mers composed of wild type and mutant subunits to study Trp binding to TRAP and its role in activating RNA binding. *J. Biol. Chem.* **2002**, *277*, 35567–35573.
- (9) McElroy, C.; Manfredo, A.; Wendt, A.; Gollnick, P.; Foster, M. TROSY-NMR studies of the 91 kDa TRAP protein reveal allosteric control of a gene regulatory protein by ligand-altered flexibility. *J. Mol. Biol.* **2002**, *323*, 463–473.
- (10) Murtola, T.; Vattulainen, I.; Falck, E. Insights into activation and RNA binding of Trp RNA-binding attenuation protein (TRAP) through all-atom simulations. *Proteins: Struct., Funct., Bioinf.* **2008**, *71*, 1995–2011.
- (11) Humphrey, W.; Dalke, A.; Schulten, K. VMD-visual molecular dynamics. *J. Mol. Graph.* **1996**, *14*, 33–38.
- (12) *Normal mode analysis: theory and applications to biological and chemical systems*; Cui, Q., Bahar, I., Ed.; Chapman and Hall/CRC: Boca Raton, FL 2006.
- (13) Skjaerven, L.; Hollup, S. M.; Reuter, N. Normal mode analysis for proteins. *J. Mol. Struct. Theochem* **2009**, *898*, 42–48.
- (14) Go, N.; Noguti, T.; Nishikawa, T. Dynamics of a small globular proteins in terms of low-frequency vibrational modes. *Proc. Natl. Acad. Sci. U.S.A.* **1983**, *80*, 3696–3700.
- (15) Brooks, B. R.; Karplus, M. Harmonic dynamics of proteins: normal mode and fluctuations in bovine pancreatic trypsin inhibitor. *Proc. Natl. Acad. Sci. U.S.A.* **1983**, *80*, 6571–6575.
- (16) Gibrat, J. F.; Go, N. Normal mode analysis of human lysozyme: study of the relative motion of the two domains and characterization of the harmonic motion. *Proteins* **1990**, *8*, 258–279.
- (17) Brooks, B. R.; Karplus, M. Normal modes for specific motions of macromolecules: application to the hinge-bending mode of lysozyme. *Proc. Natl. Acad. Sci. U.S.A.* **1985**, *82*, 4995–4999.

- (18) Thomas, A.; Field, M. J.; Mouawad, L.; Perahia, D. Analysis of the low frequency normal modes of the T-state of aspartate transcarbamylase. *J. Mol. Biol.* **1996**, *257*, 1070–1087.
- (19) Tama, F.; Valle, M.; Frank, J.; Brooks, C. L. Dynamic reorganization of the functionally active ribosome explored by normal mode analysis and cryo-electron microscopy. *Proc. Natl. Acad. Sci. U.S.A.* **2003**, *100*, 9319–9323.
- (20) Bertaccini, E. J.; Trudell, J. R.; Lindahl, E. Normal-mode analysis of the glycine alpha1 receptor by three separate methods. *J. Chem. Inf. Model.* **2007**, *47*, 1572–1579.
- (21) Gaillard, T.; Martin, E.; Sebastian, E. S.; Cossio, F. P.; Lopez, X.; Dejaegere, A.; Stote, R. H. Comparative normal mode analysis of LFA-1 integrin I-domains. *J. Mol. Biol.* **2007**, *374*, 231–249.
- (22) Tirion, M. M. Large amplitude elastic motions in proteins from a single-parameter, atomic analysis. *Phys. Rev. Lett.* **1996**, *77*, 1905–1908.
- (23) Haliloglu, T.; Bahar, I.; Erman, B. Gaussian dynamics of folded proteins. *Phys. Rev. Lett.* **1997**, *79*, 3090–3093.
- (24) Lu, M.; Ma, J. The role of shape in determining molecular motions. *Biophys. J.* **2005**, *89*, 2395–2401.
- (25) Tama, F.; Brooks, C. L. Symmetry, form, and shape: guiding principles for robustness in macromolecular machines. *Annu. Rev. Biophys. Biomol.* **2006**, *35*, 115–133.
- (26) Jordan, P. C.; Miloshevsky, G. V.; Hassanein, A. Shape-dependent global deformation modes of large protein structures. *J. Mol. Struct.* **2010**, *972*, 41–50.
- (27) Mory, T.; Kokubo, H.; Shimizu, H.; Iwamoto, M.; Oiki, S.; Okamoto, Y. Normal mode analysis of Polytheonamide B. *J. Phys. Soc. Jpn.* **2007**, *76*, 094801–1–10.
- (28) van Vlijmen, H. W. T.; Karplus, M. Normal mode calculations of icosahedral viruses with full dihedral flexibility by use of molecular symmetry. *J. Mol. Biol.* **2005**, *350*, 528–532.
- (29) Tama, F.; Brooks, C. L. Diversity and identity of mechanical properties of icosahedral viral capsids studied with elastic network normal mode analysis. *J. Mol. Biol.* **2005**, *345*, 299–314.
- (30) Simonson, T.; Perahia, D. Normal-modes of symmetrical protein assemblies: application to the tobacco mosaic-virus protein disk. *Biophys. J.* **1992**, *61*, 410–427.
- (31) Kim, M. K.; Jernigan, R. L.; Chirikjian, G. S. An elastic network model of HK97 capsid maturation. *J. Struct. Biol.* **2003**, *143*, 107–117.
- (32) Peeters, K.; Taormina, A. Group theory of icosahedral virus capsid vibrations: A top-down approach. *J. Theor. Biol.* **2009**, *256*, 607–624.
- (33) Wynsberghe, A. W. V.; Cui, Q. Interpreting correlated motions using normal mode analysis. *Structure* **2006**, *14*, 1647–1653.
- (34) Hess, B.; Kutzner, C.; van der Spoel, D.; Lindahl, E. GROMACS 4: Algorithms for highly efficient, load-balanced, and scalable molecular simulation. *J. Chem. Theory Comput.* **2008**, *4*, 435–447.
- (35) Duan, Y.; Wu, C.; Chowdhury, S.; Lee, M. C.; Xiong, G. M.; Zhang, W.; Yang, R.; Cieplak, P.; Luo, R.; Lee, T.; Caldwell, J.; Wang, J. M.; Kollman, P. A point-charge force field for molecular mechanics simulations of proteins based on condensed-phase quantum mechanical calculations. *J. Comput. Chem.* **2003**, *24*, 1999–2012.
- (36) Cheatham, T. E., 3rd; Cieplak, P.; Kollman, P. A. A modified version of the Cornell et al. force field with improved sugar pucker phases and helical repeat. *J. Biomol. Struct. Dyn.* **1999**, *16*, 845–862.
- (37) Lindahl, E.; Azuara, C.; Koehl, P. Delarue, Marc. NOMAD-Ref: visualization, deformation and refinement of macromolecular structures based on all-atom normal mode analysis. *Nucleic Acids Res.* **2006**, *34*, 52–56.
- (38) Ichiye, T.; Karplus, M. Collective motions in proteins: a covariance analysis of atomic fluctuations in molecular dynamics and normal mode simulations. *Proteins* **1991**, *11*, 205–217.
- (39) Niv, M. Y.; Filizola, M. Influence of oligomerization on the dynamics of G-protein coupled receptors as assessed by normal mode analysis. *Proteins: Struct., Funct., Bioinf.* **2008**, *71*, 575–586.
- (40) Wynsberghe, A. V.; Li, Guohui.; Cui, Q. Normal-mode analysis suggests protein flexibility modulation throughout RNA polymerase's functional cycle. *Biochemistry* **2004**, *43*, 13083–13096.
- (41) Dobbins, S. E.; Lesk, V. I.; Sternberg, M. J. Insights into protein flexibility: the relationship between normal modes and conformational change upon protein–protein docking. *Proc. Natl. Acad. Sci. U.S.A.* **2008**, *105*, 10390–10395.
- (42) Hayward, S.; Kitao, A.; Go, N. Harmonic and anharmonic aspects in the dynamics of PBTI: A normal mode analysis and principal component analysis. *Protein Sci.* **1994**, *3*, 936–943.
- (43) Hayward, S.; Go, N. Annu. Collective variable description of native protein dynamics. *Rev. Phys. Chem.* **1995**, *46*, 223–250.
- (44) Ceulemans, A.; Vos, I. The vibrations of annular and globular molecules - theory. *Mol. Phys.* **1991**, *72*, 1051–1080.
- (45) Bertaccini, E. J.; Lindahl, E.; Sixma, T.; Trudell, J. R. Effect of cobratoxin binding on the normal mode vibration within acetylcholine binding protein. *J. Chem. Inf. Model.* **2008**, *48*, 855–860.
- (46) Ceulemans, A.; Chibotaru, L. F.; Fowler, P. W. Molecular anapole moments. *Phys. Rev. Lett.* **1998**, *80*, 1861–1864.
- (47) Fowler, P. W.; Rassat, A.; Ceulemans, A. Symmetry generalization of the Euler-Schlafli theorem for multi-shell polyhedra. *J. Chem. Soc., Faraday Trans.* **1996**, *92*, 4877–4884.
- (48) Thirumuruganandham, S. P.; Urbassek, H. M. Low-frequency vibrational modes and infrared absorbance of red, blue and green opsins. *J. Mol. Model.* **2009**, *15*, 959–969.
- (49) Cheng, S.; Niv, M. Y. Molecular dynamics simulations and elastic network analysis of protein Kinase B (Akt/PKB) inactivation. *J. Chem. Inf. Model.* **2010**, *50*, 1602–1610.
- (50) Skjaerven, L.; Martinez, A.; Reuter, N. Principal component and normal mode analysis of proteins: a quantitative comparison using the GroEL subunit. *Proteins: Struct., Funct., Bioinf.* **2011**, *79*, 232–243.
- (51) Tama, F.; Gadea, F. X.; Marques, O.; Sanejouand, Y. H. Building-block approach for determining low-frequency normal modes of macromolecules. *Proteins: Struct. Funct. Genet.* **2000**, *41*, 1–7.
- (52) Ghysels, A.; Van Speybroeck, V.; Pauwels, E.; Catak, S.; Brooks, B. R.; Van Neck, D.; Waroquier, M. Comparative study of various normal mode analysis techniques based on partial Hessians. *J. Comput. Chem.* **2010**, *31*, 994–1007.
- (53) Bahar, I. Perspectives on: Molecular dynamics and computational methods: On the functional significance of soft modes predicted by coarse-grained models for membrane proteins. *J. Gen. Physiol.* **2010**, *135*, 563–573.
- (54) Taly, A.; Delarue, M.; Grutter, T.; Nilges, M.; Le Novere, N.; Corringer, P. J.; Changeux, J. P. Normal mode analysis suggests a quaternary twist model for the nicotinic receptor gating mechanism. *Biophys. J.* **2005**, *88*, 3954–3965.
- (55) Shrivastava, I. H.; Bahar, I. Common mechanism of pore opening shared by five different potassium channels. *Biophys. J.* **2006**, *90*, 3929–3240.